Eur. Phys. J. D (2012) 66: 182
DOI: 10.1140/epjd/e2012-30204-4

THE EUROPEAN PHYSICAL JOURNAL D

Regular Article

Dark lattice solitons in one-dimensional waveguide arrays with defocusing saturable nonlinearity and alternating couplings

A. Kanshu[1], C.E. Rüter[1], D. Kip[1], J. Cuevas[2,a], and P.G. Kevrekidis[3]

[1] Faculty of Electrical Engineering, Helmut Schmidt University, 22043 Hamburg, Germany
[2] Grupo de Física No Lineal, Departamento de Física Aplicada I, Universidad de Sevilla, Escuela Politécnica Superior, C/Virgen de África 7, 41011 Sevilla, Spain
[3] Department of Mathematics and Statistics, University of Massachusetts, MA 01003-4515 Amherst, USA

Received 28 March 2012 / Received in final form 3 May 2012
Published online 12 July 2012 – © EDP Sciences, Società Italiana di Fisica, Springer-Verlag 2012

Abstract. In the present work, we examine "binary" waveguide arrays, where the coupling between adjacent sites alternates between two distinct values C_1 and C_2 and a saturable nonlinearity is present on each site. Motivated by experimental investigations of this type of system in fabricated $LiNbO_3$ arrays, we proceed to analyze the nonlinear wave excitations arising in the self-defocusing nonlinear regime, examining, in particular, dark solitons and bubbles. We find that such solutions may, in fact, possess a reasonably wide, experimentally relevant parametric interval of stability, while they may also feature both prototypical types of instabilities, namely exponential and oscillatory ones, for the same configuration. The dynamical manifestation of the instabilities is also examined through direct numerical simulations.

1 Introduction

Dark solitary waves are ubiquitous nonlinear excitations of dispersive wave models with a so-called self-defocusing nonlinearity. Perhaps the prototypical model where they arise is the nonlinear Schrödinger equation with a defocusing nonlinearity [1], as it is referred to in nonlinear optics (since it induces the spreading of optical beams). These excitations consist of a density dip (i.e., a dark notch) accompanied by a phase jump across the density minimum. In addition to their observation in nonlinear optics extensively summarized in [1,2], numerous experiments have demonstrated the emergence of these nonlinear states in the atomic physics of Bose-Einstein condensates, as has recently been comprehensively reviewed in [3]. Interestingly, the physical relevance of dark solitons is not limited to these areas, but rather also extends to parametrically-driven shallow liquids [4], discrete mechanical systems [5], electrical lattices with nonlinear capacitors [6], thin magnetic films [7] and dissipative variants thereof in complex plasmas [8], among others.

In recent years, there has been a considerable interest in the realization of such excitations in systems bearing lattice potentials, to appreciate the effects of discreteness on the existence and stability, as well as on the dynamics and mobility of such excitations; see e.g. the prototypical theoretical study of [9] and even the earlier work of [10]. Experimental developments have enabled the realization of such excitations, especially so in arrays of optical waveguides either in the context of AlGaAs in the anomalous diffraction regime with the cubic nonlinearity due to the Kerr effect [11], or in defocusing lithium niobate waveguide arrays, which exhibit a different type of nonlinearity, namely a saturable, defocusing one due to the photovoltaic effect [12]. These experimental investigations, in turn, led to comparative studies between the features of the dark solitons in these two discrete models [13,14], as well as to the examination of states consisting of multiple dark solitary waves [15,16]. These findings have been summarized in a recent book [17]. Furthermore, in these waveguide array systems, not only have dark solitons been identified in higher gaps (of the associated periodic potentials) [18], but they have also been found to arise as members of multi-component soliton complexes such as dark-bright solitary waves [19].

In the present work, we consider a nontrivial variant of the above nonlinear dynamical lattices. In particular, we focus on the setting of "heterogeneous" lattices and more specifically in the context of lattices with alternating couplings between two distinct values C_1 and C_2. The existence and stability of bright solitons in binary lattices has been investigated both theoretically [20,21] and experimentally [22,23]. It should be added, however, that binary lattices can be constructed in different ways, such as e.g. by waveguides of the same separation between the channels, but alternating in widths as in [22], or by ones

[a] e-mail: jcuevas@us.es

of the same width but alternating in separation as in [23]. Here, in line with the latter approach, we fabricate one-dimensional arrays of such lattices in a nominally non-doped $LiNbO_3$ substrate by Ti in-diffusion. In this case the underlying linear spectrum possesses two pass bands, with a mini-gap between them (as opposed to the single band of the homogeneous waveguide array). In the gaps of the linear spectrum, we will seek nonlinear wave solutions, such as dark solitons and bubbles in what follows. We find that both types of obtained nonlinear waves may possess both regions of stability as well as regions of both types of instability, exponential as well as oscillatory, as the propagation constant parameter is varied. This is contrary to what is the case for the homogeneous (coupling) counterpart of the model, where only oscillatory (or only exponential) instabilities may be observed for a particular type of configuration. When the waveforms are found to be unstable, direct numerical simulations of the system are used to explore the evolution of the instability, giving rise to the breakup of the stationary structure into moving states or to its breathing dynamics.

Our presentation is structured as follows. In Section 2, we present the experimental setup and some prototypical experimental results. These, in turn, motivate the theoretical model presentation and discussion of Section 3 and the systematic numerical investigation of Section 4. Finally, in Section 5, we summarize our findings and propose some potential directions for future study.

2 Experimental motivation

For our experiments, we fabricate a one-dimensional waveguide array in a nominally non-doped $LiNbO_3$ substrate. Using standard photolithographic techniques, we form, on the substrate's surface, an array with 250 Ti stripes of equal width $W = 4.0$ μm and alternating distances $d_1 = 2.5$ μm and $d_2 = 4.5$ μm between them. By in-diffusion of Ti stripes at $T = 1000$ °C and following polishing, we obtain samples with dimensions of 1 mm × 20 mm × 7.8 mm, where the ferroelectric c-axis is pointing along the 7.8 mm-long direction, and channels are aligned along the 20 mm-long propagation direction (Fig. 1a). By choosing an appropriate thickness of the sputtered Ti stripes, and duration and temperature of in-diffusion, we form a sample possessing only a single allowed band (Figs. 1b–1d). This allows us to use standard end-facet coupling for studying linear and nonlinear light propagation in the lattice. Contrary to the single uniform lattice, the first band of our sample is split into two parts, separated by an additional mini-gap that opens in the middle of the Brillouin zone. Finally, this sample possesses a defocusing saturable nonlinearity which is probably due to small impurity concentrations incorporated into the substrate during high-temperature treatment, as well as intrinsic photorefractive defects like Nb on Li sites in congruently melting $LiNbO_3$. At slightly higher intensities or input powers (of the order of (10–100) μW per channel) the observed nonlinear index changes of this sample are of approximately the same magnitude when compared to, for example, those fabricated on Fe-doped substrates.

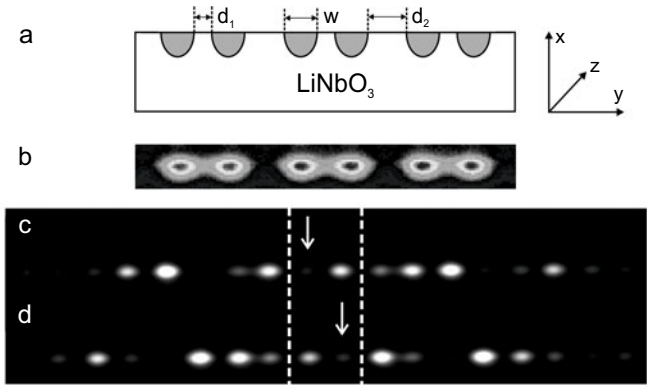

Fig. 1. Geometry of the binary waveguide array (a), experimental output intensity distribution for homogeneous array excitation with Bloch momentum $k = 0$ (b), output intensity distribution when a single element of the binary lattice is excited (see arrows), either on the left (c) or the right hand side (d).

To form dark solitons in our sample, we focus an appropriate light amplitude distribution onto the polished input facet, and record the temporal evolution of the out-coupled light by means of a 20 × microscope objective and a CCD camera connected to a computer. With the help of an additional plane reference wave we are able to monitor the phase distribution of the out-coupled light, too. For the case of a binary lattice different kinds of dark soliton solutions exist: a fundamental dark soliton in the semi-infinite gap, a bubble-like dark soliton that is located in the semi-infinite gap, too, and another dark soliton existing in the extra mini-gap having an alternating phase distribution. All solutions require excitation using a suitable amplitude profile and appropriate power to be formed. Because the nonlinearity of our sample is of saturable nature, we can, in a certain range, vary the input light power accordingly in order to generate the necessary nonlinear index changes for dark soliton formation.

For the formation of a dark soliton in the semi-infinite gap above the center of the Brillouin zone at $k = 0$, we use a broad input beam (diameter 6 mm) of wavelength 532 nm with homogeneous intensity distribution that is focused into the lattice with the help of a cylindrical lens ($f = 100$ mm). This beam passes a phase mask (half-wave MgF_2 layer evaporated on glass substrate) which imparts an additional phase of π on half of the beam. The dark notch generated in this way is adjusted to coincide with the center of one element of the binary lattice. First, in Figure 2a we show the output intensity distribution, when the lattice is excited on the input surface homogeneously without using the phase mask. Adding the phase mask into the beam and using low input powers of the order of nW, we observe discrete diffraction of the generated dark notch in Figure 2b. With increasing power, the sample starts to behave nonlinearly and the width of the dark notch decreases with increasing recording time.

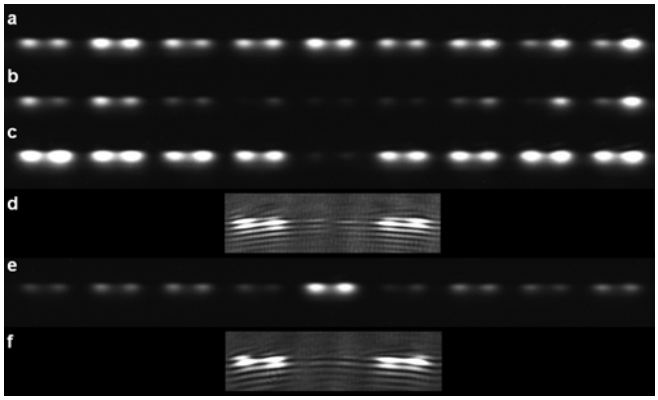

Fig. 2. Light distribution on the output surface of the lattice by homogeneous excitation on input surface (a), discrete diffraction (b), dark soliton (c), interferogram of the dark soliton showing the π phase jump (d), guiding properties of a dark soliton when the lattice is excited with a homogeneous probe beam (e), and interferogram of a bubble soliton when both sides of the dark notch are in phase (f).

After a few minutes it evolves finally into a dark soliton shown in Figure 2c, where the width of the dark notch matches the one on the input facet. This nonlinear state is robust and can be observed for more than one hour without noticeable changes. The corresponding phase relation is demonstrated in the interferogram presented in Figure 2d, which clearly shows the phase jump of π in the center of the structure. The generation of a dark soliton leads to a change of the corresponding refractive index profile and the formation of a positive defect located at the position of the dark notch. We test the guiding properties of this defect by launching a broad probe beam of low intensity having a plane phase front, and observe trapping of light inside the recorded defect in Figure 2e. The experimental setup used in this work is similar to the one in reference [12], but with the two-beam interference on the input side replaced by a phase mask.

When the phase mask used to add the extra phase jump of π on the input light distribution is misadjusted (tilted), a dark notch (generated in part by a shadow region induced by the mask) with both sides of the structure being in phase is formed. Using this input light distribution on the input facet, we are able to experimentally observe another nonlinear localized mode: the generated bubble solution has a similar intensity distribution as the dark soliton (Fig. 2c), but without a phase jump of π in the center. The corresponding phase distribution on the output facet is given in Figure 2f. Note that in the experiment this nonlinear state is found to be unstable for long recording time, but may be observed during the initial time of recording only. For longer recording or when the input power is further increased, a transformation to the dark soliton solution described previously occurs. This experimental observation suggests that the dark soliton should be structurally more robust than the bubble waveform.

To form a dark soliton in the mini-gap one needs to excite each dimer of the lattice in phase, with alternating phase jumps between neighboring units. Additionaly, a π phase jump inside the central element is required to generate a dark notch. By using an interference pattern with a modulation adjusted to fit to the grating period of our lattice, and by passing this beam through an additional phase mask for the generation of the dark notch, a suitable input light distribution has been generated. However, due to limited precision in the adjustment (this was mainly the limited symmetry in exciting each dimer with exactly equal powers in both channels), no clear discrete diffraction pattern was observed for this situation on the output. Thus, we were unable to perform the corresponding nonlinear experiments. A possible solution might be the use of a spatial light modulator to create a more precisely defined input profile, which was not available presently in the experimental setup used. It should be noted here that these "staggered" states have, in fact, been accessible to our numerical investigations. Nevertheless, the lack of experimental control over their generation indicated above, as well as equally importantly, our generic observation of their large scale instability and the rapid evolution of their unstable background towards lattice dynamical turbulence have precluded us from considering these states further herein.

3 Theoretical model and analytical considerations

In order to theoretically model a setup corresponding to our experimental configuration, we consider a set of discrete nonlinear Schrödinger (DNLS) equations with a saturable onsite nonlinearity (see also [12]) in the form:

$$i\frac{dA_j}{dz} + (C_1 B_j + C_2 B_{j-1}) + \alpha \frac{|A_j|^2}{1+\kappa|A_j|^2} A_j = 0, \quad (1)$$

$$i\frac{dB_j}{dz} + (C_1 A_j + C_2 A_{j+1}) + \alpha \frac{|B_j|^2}{1+\kappa|B_j|^2} B_j = 0. \quad (2)$$

The defocusing nature of the nonlinearity is encapsulated in the value of $\alpha = -1$; furthermore, we have used a value of $\kappa = 5 \times 10^{-4}$ which has been found to accurately account for the saturation effect. The electric field of interest E_n is defined from A_j and B_j as:

$$E_{2j} = A_j, \qquad E_{2j+1} = B_j. \quad (3)$$

Within this model, we seek stationary solutions in the form:

$$A_n = \exp(i\beta z) a_n, \qquad B_n = \exp(i\beta z) b_n. \quad (4)$$

For the experimental waveguide array, by matching information about the linear diffraction properties of the lattice, we have inferred that $C_1 = 0.43$ mm^{-1} and $C_2 = 0.14$ mm^{-1} provide reasonable approximations to the experimental diffraction pattern observations

(see Figs. 1c and 1d). In light of that, we have fixed the value of C_1 to 0.43 mm^{-1}, but in order to appreciate the effect of variation of the spacing, we have looked at the relevant phenomenology as a function of the parameter C_2. Furthermore, we have varied the propagation constant β, in order to explore the family of nonlinear stationary, potentially observable solutions.

We have focused, in particular, on two different types of solutions, namely dark [14,15] and bubble [24] solitons, chiefly with a uniform background and $a_n, b_n \in \mathbb{R}\,\forall n$.

Upon identifying the relevant solutions through a fixed point computation, we have proceeded to examine their spectral stability properties by considering a linearization analysis. To that effect, small perturbations [of order $\mathrm{O}(\delta)$, with $0 < \delta \ll 1$] are introduced in the form

$$A_n(z,x) = e^{i\beta z}\left[A_{n,0} + \delta(P_n e^{i\omega z} + Q_n^* e^{-i\omega^* z})\right],$$
$$B_n(z,x) = e^{i\beta z}\left[B_{n,0} + \delta(R_n e^{i\omega z} + S_n^* e^{-i\omega^* z})\right], \quad (5)$$

and the ensuing linearized equations are then solved to $\mathrm{O}(\delta)$, leading to the following eigenvalue problem:

$$\omega\begin{pmatrix} P_n \\ Q_n \\ R_n \\ S_n \end{pmatrix} = \begin{pmatrix} L_1(a_{n,0}) & L_2(a_{n,0}) & H_n^- & 0 \\ -L_2(a_{n,0}) & -L_1(a_{n,0}) & 0 & -H_n^- \\ H_n^+ & 0 & L_1(b_{n,0}) & L_2(b_{n,0}) \\ 0 & -H_n^+ & -L_2(b_{n,0}) & -L_1(b_{n,0}) \end{pmatrix} \times \begin{pmatrix} P_n \\ Q_n \\ R_n \\ S_n \end{pmatrix}, \quad (6)$$

for the eigenfrequency ω and the associated eigenvector $(P_n, Q_n, R_n, S_n)^T$, where L_1, L_2, $H_n^\pm$ are the following operators:

$$L_1(x) = \beta + \nu\frac{2|x|^2 + |x|^4}{(1+|x|^2)^2},$$
$$L_2(x) = \nu\frac{x^2}{(1+|x|^2)^2},$$
$$H_n^\pm x_n = C_1 x_n + C_2 x_{n\pm1}.$$

and with

$$\nu = \frac{\alpha}{\kappa} \times 10^{-3} = -2. \quad (7)$$

As the relevant solutions (stationary dark solitons which possess a phase jump across the density dip, as well as bubbles with no phase jump across the dip) live against the backdrop of a constant density background, it is relevant to examine the linearization properties of such a background. This can be done by using the following form:

$$a_n = \phi\exp(ikn), \qquad b_n = \phi\exp(ikn), \quad (8)$$

with k being the wavenumber of the background. In our case, we have restricted our considerations to $k = 0$ (unstaggered background) and $k = \pi$ (staggered background). Introducing the relation above into equation (4) we get:

$$\beta = -\nu\frac{\phi^2}{1+\phi^2} - \epsilon(k), \quad (9)$$

where $\epsilon(k) = C_1 + C_2\cos(k)$. It is important to note here that in order that $\phi \in \mathbb{R}$, the condition that needs to be fulfilled reads:

$$\beta \in [-\epsilon(k), -\nu - \epsilon(k)], \quad (10)$$

which, when $k = 0$, will turn out (in our numerical results below) to coincide with the existence interval for dark solitons with unstaggered background. More generally, that condition constitutes a necessary one for the existence of dark/bubble solitons. In fact, as we will see below bubble solutions only exist in a sub-interval of the allowable parametric interval.

The dispersion relation of the linear excitations corresponds to the continuous spectrum that will be identified in the linearization around our solitary wave solutions. This relation can be identified by decomposing the perturbations as $\{P_n, Q_n, R_n, S_n\} = \{P, Q, R, S\}\exp(iqn)$ in equation (4) and deriving the resulting condition:

$$\omega_\pm^2(q) = \epsilon(k)[\epsilon(k) - 2h(k)] + g^2(q) \pm 2[h(k) - \epsilon(k)]g(q) \quad (11)$$

with

$$h(k) = -\frac{[\beta + \epsilon(k)][\nu + \beta + \epsilon(k)]}{\nu}, \quad (12)$$
$$g^2(q) = C_1^2 + C_2^2 + 2C_1C_2\cos(q). \quad (13)$$

It is easy to check that equation (11) predicts the existence, when restricting to positive eigenfrequencies, of two bands of real eigenvalues $\omega_\pm$ when $k = 0$; besides, that equation also predicts for $k = \pi$ the existence of a band ω_- with real eigenfrequencies and another band ω_+ with imaginary eigenfrequencies. This amounts to the modulational instability of the background [25] which is detrimental for the survival of the staggered states mentioned in the previous section.

4 Numerical observations

We now turn to numerical observations, as a way of illustrating the existence and potential stability of the localized states under consideration above.

Figures 3, 4 show examples of the profile and the spectral stability planes of dark and bubble solitons with unstaggered backgrounds. It can be seen that as the propagation parameter is varied, the discrete dark soliton solution may go from a regime of spectral stability to one of weak oscillatory instability and finally to one of stronger exponential instability. The former (oscillatory) instability is associated with complex eigenfrequencies, while the latter (exponential) instability with purely imaginary ones. Similar features are observed for the bubbles presented in Figure 4. A fundamental difference appears to be that for

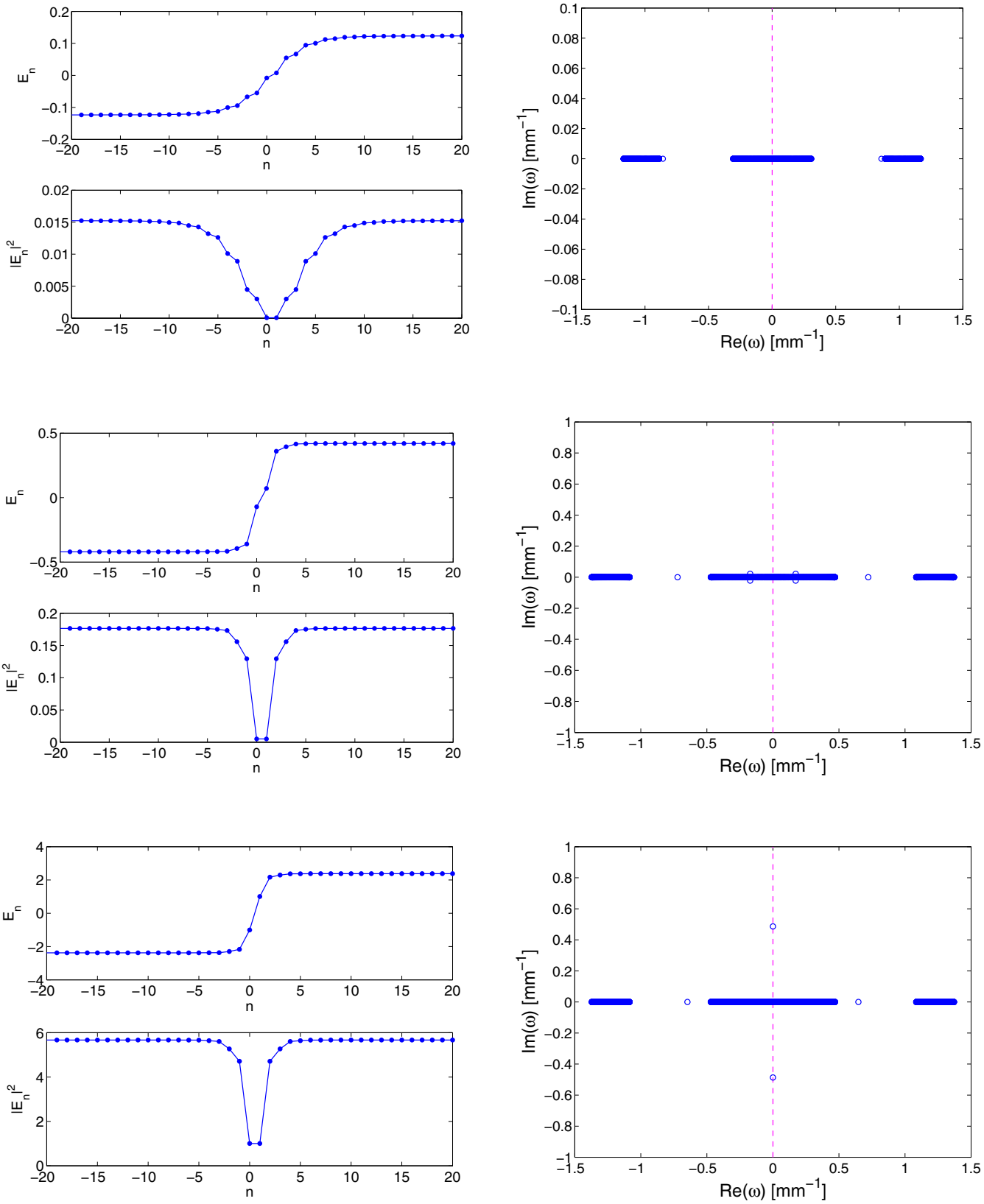

Fig. 3. (Color online) (Left) Profile of the normalized electric field and the corresponding intensity pattern for a dark soliton with $C_2 = 0.14$ and $\beta = -0.54$ (top), $\beta = -0.27$ (middle) and $\beta = 1.13$ (bottom). The corresponding right panels show the spectral stability plane. In the latter, the existence of eigenfrequencies with non-vanishing imaginary part is tantamount to instability with a growth rate equal to the absolute value of this imaginary part.

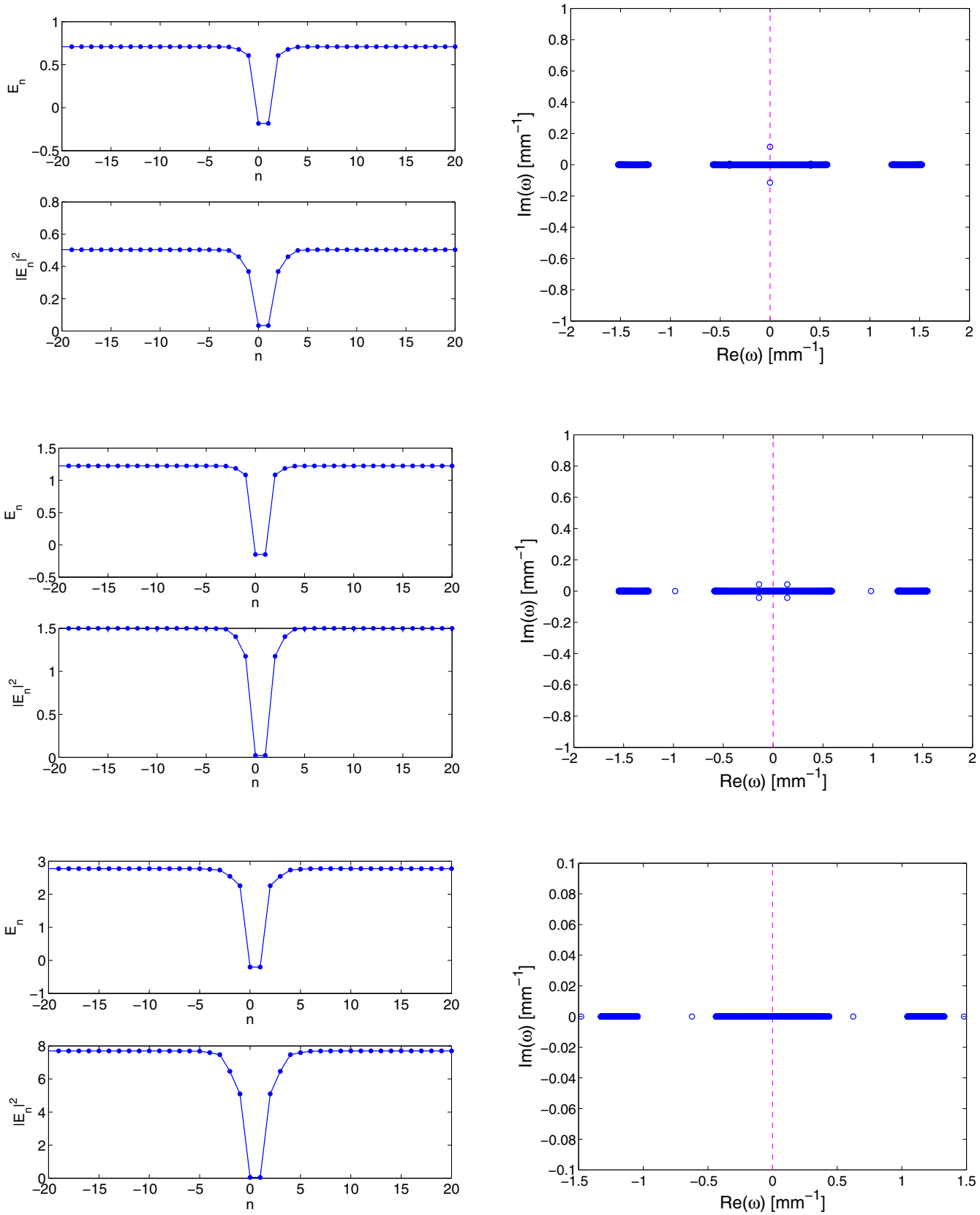

Fig. 4. (Color online) (Left) Profile of the normalized electric field and the corresponding intensity pattern for a bubble soliton with $C_2 = 0.14$ and $\beta = 0.10$ (top panel), $\beta = 0.63$ (middle panel) as well as $\beta = 1.2$ (bottom panel). The corresponding right panels show the spectral stability plane.

dark solitons an eigenfrequency pair associated with the wave first moves along the real frequency axis. This leads to resonances with the modes of the continuous spectrum, yielding oscillatory instabilities until a point of maximal excursion i.e., maximal Re(ω). Thereafter, the real part of this eigenfrequency starts decreasing and eventually crosses zero. Thus, it becomes unstable as an imaginary eigenfrequency causing an exponential instability. On the contrary, the relevant eigenfrequency pair first becomes imaginary for bubbles, leading to an immediate exponential instability. Then, upon a maximal excursion, it returns to the origin, and subsequently moves along the real frequency axis. This gives rise to an oscillatory instability (although additional oscillatory instabilities may also exist). These features are presented for different values of C_2 in Figure 5. It is relevant to mention that in that figure in addition to the experimentally relevant value of $C_2 = 0.14$, presented both for dark solitons (top panel) and for bubbles (bottom panel), cases of considerably smaller and larger C_2 are examined in the middle panels. For smaller C_2, the range of oscillatory instabilities shrinks (chiefly because of the narrower interval of continuous spectrum and the wider spectral gap in such a case). On the other hand, for larger C_2, the corresponding instability is exponential and is found to arise throughout the examined interval of propagation constants (see third panel of Fig. 5). More specifically, for $C_2 = 0.05$, the exponential instability in the right panel of Fig. 5) only exists for the dark solitons with $\beta \geq 0.81$; for $C_2 = 0.14$, it exists for $\beta \geq 0.48$ and for $C_2 = 0.5$, it exists for all $\beta \geq -0.92$. On the other hand, for the bubbles of the bottom right panel of the figure, the exponential instability is only present for $\beta \leq 0.54$ (notice the opposite sign of the inequality as discussed above).

The detailed existence range of dark and bubble solitons is shown in Figure 6. It is worth remarking that our numerics show that dark solitons always exist in the range $\beta \in [-(C_1 + C_2), -(C_1 + C_2 - \nu)]$; however, the existence range of bubbles is limited (to a narrower sub-interval), and these solutions cease to exist for $C_2 \geq 0.34$. The stability properties together with the relevant instability growth rates are summarized in Figure 7. It should be noted that there exist windows of stability inside the region where the solitons are oscillatorily unstable; this fact is caused by the finite lattice size (see e.g., [9] for a relevant discussion) and is ubiquitous for dark solitons in lattices. Furthermore, this phenomenon disappears in the limit where the length of the lattice tends to infinity.

In Figures 8–9, we show typical examples of the dynamical evolution of the relevant waveforms, which have been obtained by a 4th order fixed-step Runge-Kutta method. In these examples, we typically append to the unstable solutions a random perturbation of amplitude $\sim 10^{-3}$, so as to seed the instability (through the projection of this random perturbation to the most unstable eigenmode of the solution). The right panel of those figures is restricted to twice the sample length, i.e., $z = 40$ mm (in order to gauge the relevance of the reported phenomenology to the experimental observations). Our general conclusions based on these dynamical runs (as well as others not shown herein) is that in most cases, the exponential instabilities may lead to a breathing of the light intensity (i.e., $|E_n|^2$) or to a potential destruction of the pertinent dynamical state. An example of the former type is shown in the bottom panel of Figure 8 and is justified by the fact that for different values of the propagation constant β (and all other system parameters being identical), there exist other members of this family of solutions which are, in fact, dynamically stable. An example of the latter type is shown in the top panel of Figure 9 for the pertinent bubble state. On the other hand, instabilities associated with complex quartets of eigenfrequencies are found to give rise to an oscillatory growth that is eventually seen to typically lead to propagation of excitations through the lattice with a non-zero angle (i.e., moving solitary waves). An example of this type can be seen e.g. for a dark soliton in the top panel of Figure 8, while for a bubble a similar observation but leading to a more complex dynamical state can be seen in the bottom panel of Figure 9. Similar oscillatory instability evolutionary outcomes for a homogeneous lattice can be found e.g. in [10,13].

As concerns the bubbles, we should note that their dynamical instability in the cubic-quintic problem was systematically studied in the works of [27,28] through a series of analytical and numerical tools. There, it was found that stationary bubbles were unstable through a splitting towards stable traveling ones. The fundamental difference encountered here e.g. in Figure 9 with respect to that setting is that in the present work, the state of vanishing intensity is dynamically unstable and hence the instability is more likely to break up the bubble into shallower propagating excitations, rather than to an expanding nucleus of vanishing intensity. This is what is observed through the asymmetric process (seeded by random noise) in Figure 9, although it should also be added that in the presence of discreteness, the existence of the so-called Peierls-Nabarro barrier renders it unlikely that these excitations will maintain their speed due to the emission of small amplitude radiative wavepackets, as discussed e.g. in [29].

5 Conclusions

In the present work, motivated by the experimental examination of binary lattices with alternating couplings between two distinct values C_1 and C_2, we have proceeded to theoretically model and subsequently analyze such states in the context of optical waveguide arrays. The two prototypical states under consideration have been discrete dark solitons and bubble solutions. The distinctive feature between these two waveforms is the existence (for dark-solitons) or non-existence (for bubbles) of a phase jump across the density dip associated with the solution. Fixing one of the two couplings, we have chosen to vary the other coupling, as well as the propagation constant of the solution (as a measure of the nonlinearity) and to examine the existence and stability properties of such states. We have found that dark solitons exist throughout the interval (of couplings and/or of propagation constant) in which the background state is found to exist. On the other hand,

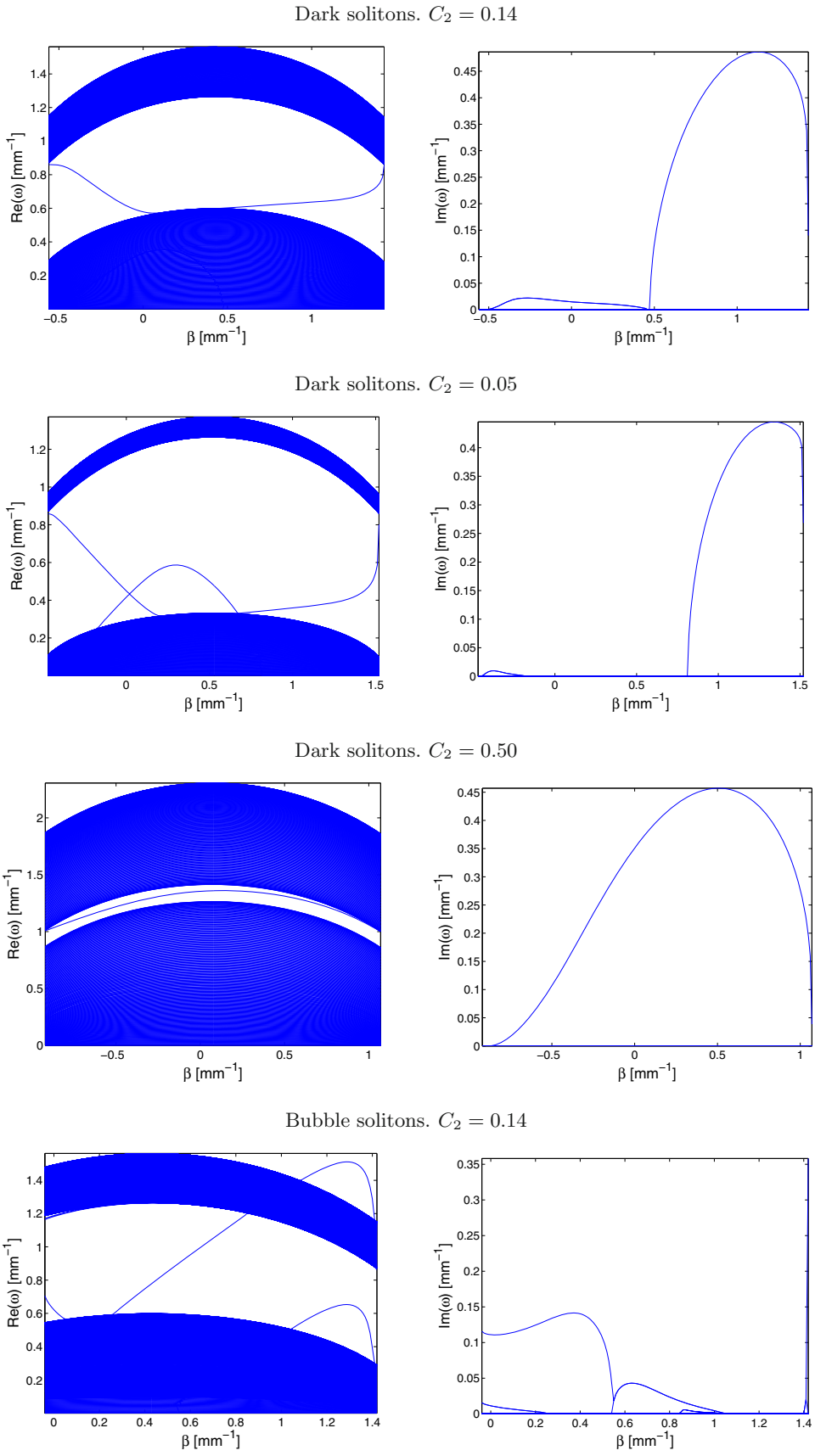

Fig. 5. (Color online) Dependence with respect to β of the real (left) and imaginary (right) part of the linearization eigenvalues for some selected values of C_2.

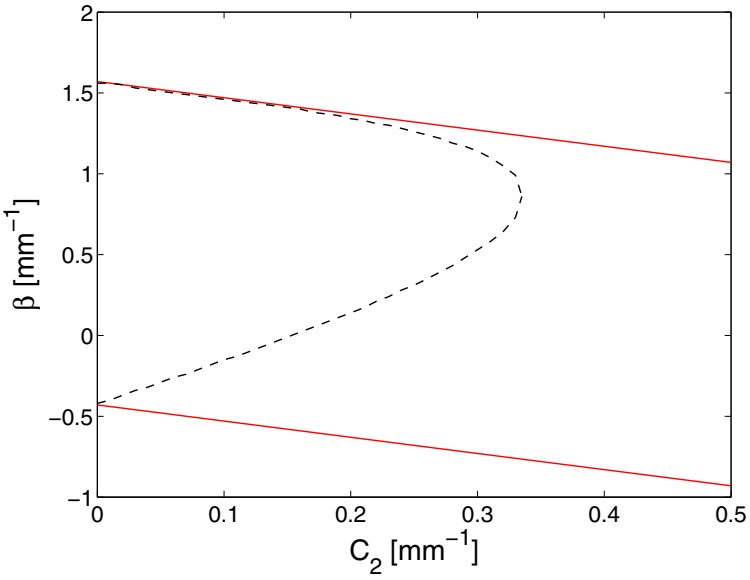

Fig. 6. (Color online) Existence range of dark solitons and bubble solitons. Dark (bubble) solitons exist in the region between the full red (dashed black) lines.

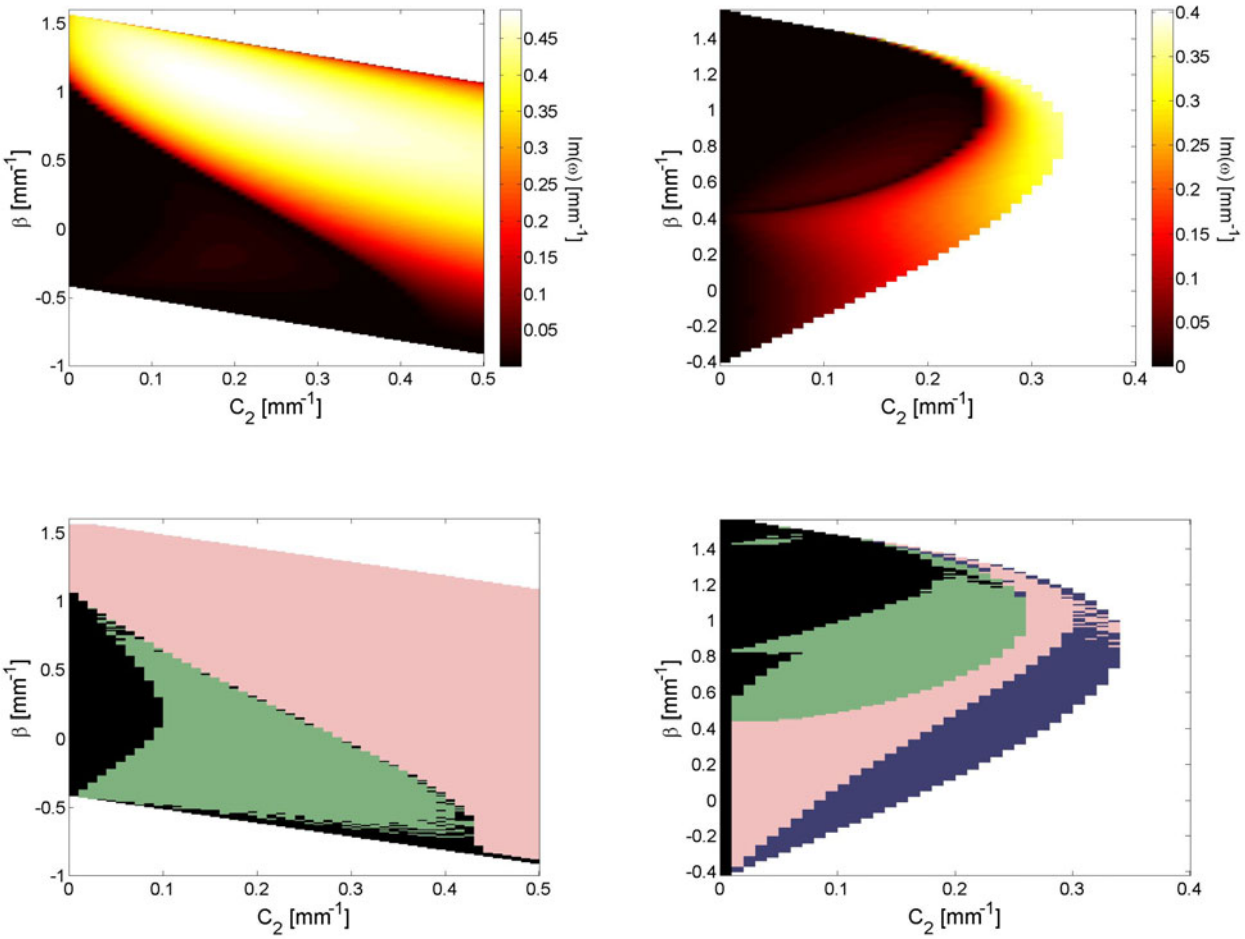

Fig. 7. (Color online) (Top panels) Instability growth rates for dark (left) and bubble (right) solitons. The bottom panels show the type of instability experienced by the solitons, with the color coding as follows: black → stability; green [medium gray] → oscillatory instability; pink [light gray] → exponential instability; blue [dark gray] → oscillatory + exponential instabilities.

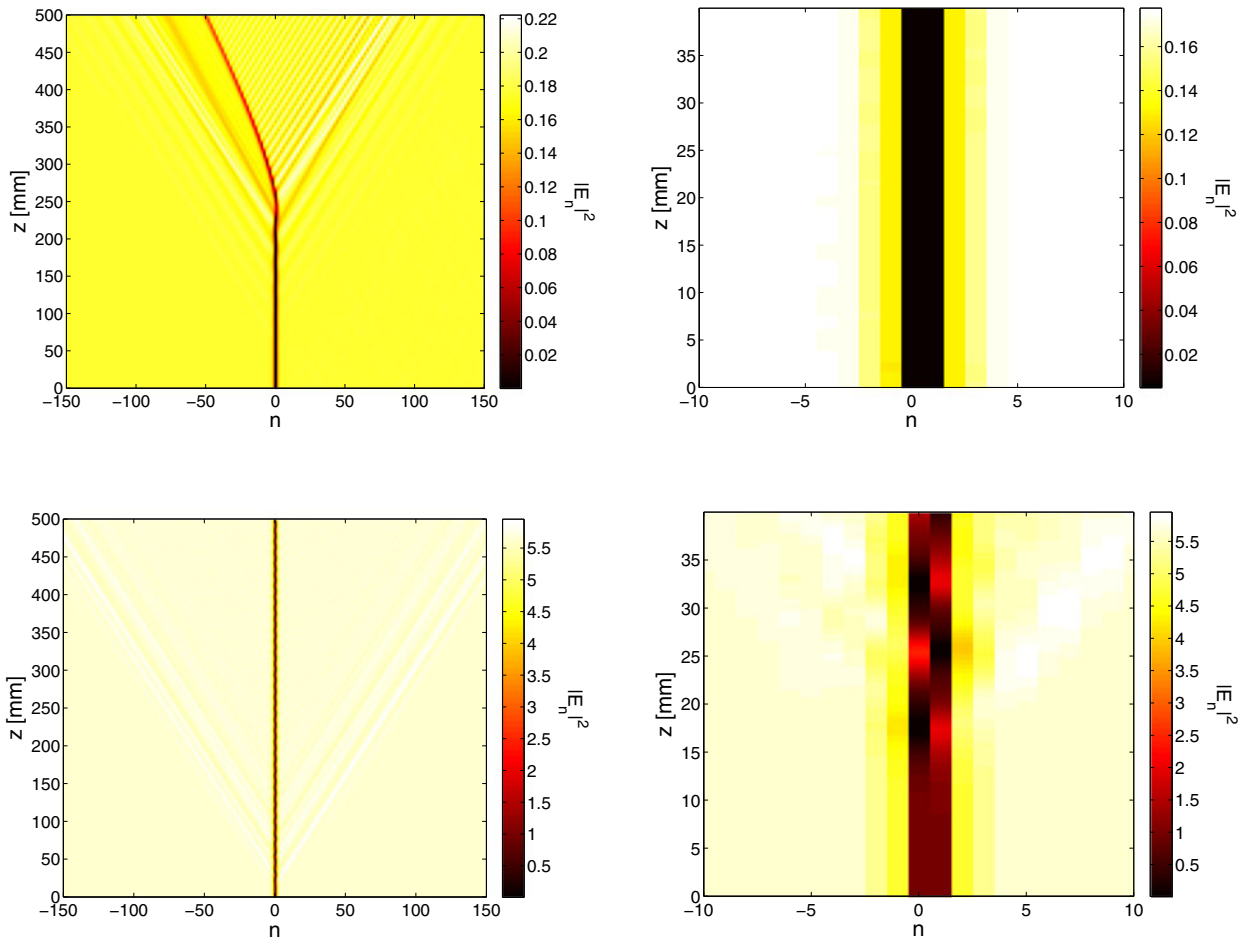

Fig. 8. (Color online) Propagation of the unstable waves of the middle and bottom panels of Figure 3, respectively, when a random perturbation of amplitude $\sim 10^{-3}$ is introduced. The right panel is a zoom of the left panel. In the left panel, the resolution of the propagation is $z = 0.1$ mm, whereas in the right panel, the resolution is $z = 0.01$ mm.

in the case of bubbles, the range of existence is found to be somewhat more limited, a feature that partially be also responsible for the experimental observation of their eventual "conversion" to dark soliton states. The existence of two tunable coupling parameters (or of the tunability of those in conjunction with the propagation constant) is found to offer some novel properties to the present model in connection to its standard homogeneous dynamical lattice counterpart. Firstly, the linear spectrum consists of two bands with a "mini-gap" between them, which is controlled by these parameters. This enables the existence of additional stationary (staggered) states whose dynamical instability has been briefly touched upon herein. Furthermore, the parameters enable transitions between oscillatory instabilities, dynamical stability and exponential instabilities for the same type of state, a wealth of possibilities that is not accessible in the standard DNLS model case.

It would be particularly interesting to extend the present considerations to higher dimensional settings and especially to two-dimensional arrays where different tunabilities of the spacings may be accessible. On the one hand, there exists the tunability between different lattice directions, essentially amounting to anisotropic nonlinear dynamical lattices (see e.g. the early examinations thereof in [26], where interesting phenomena emerged from the breaking of the perfect symmetry of the square lattice). Yet on the other hand, there is the possibility of combining this anisotropy with binary couplings, creating possibilities for inter- and intra-directional heterogeneity and their interplay. In that regard, the effect of such heterogeneous nonlinear dynamical lattices on fundamental higher dimensional excitations such as discrete vortices would be particularly interesting to explore in future work.

D.K. thanks the German Research Foundation (DFG, Grant KI 482/11-2) and the German-Israeli Foundation (GIF) for financial support of this research. P.G.K. gratefully acknowledges support from the US-NSF through grants DMS-0806762 and CMMI-1000337 and from the Alexander von Humboldt Foundation as well as the Alexander S. Onassis Public Benefit Foundation. J.C. acknowledges financial support from the MICINN project FIS2008-04848.

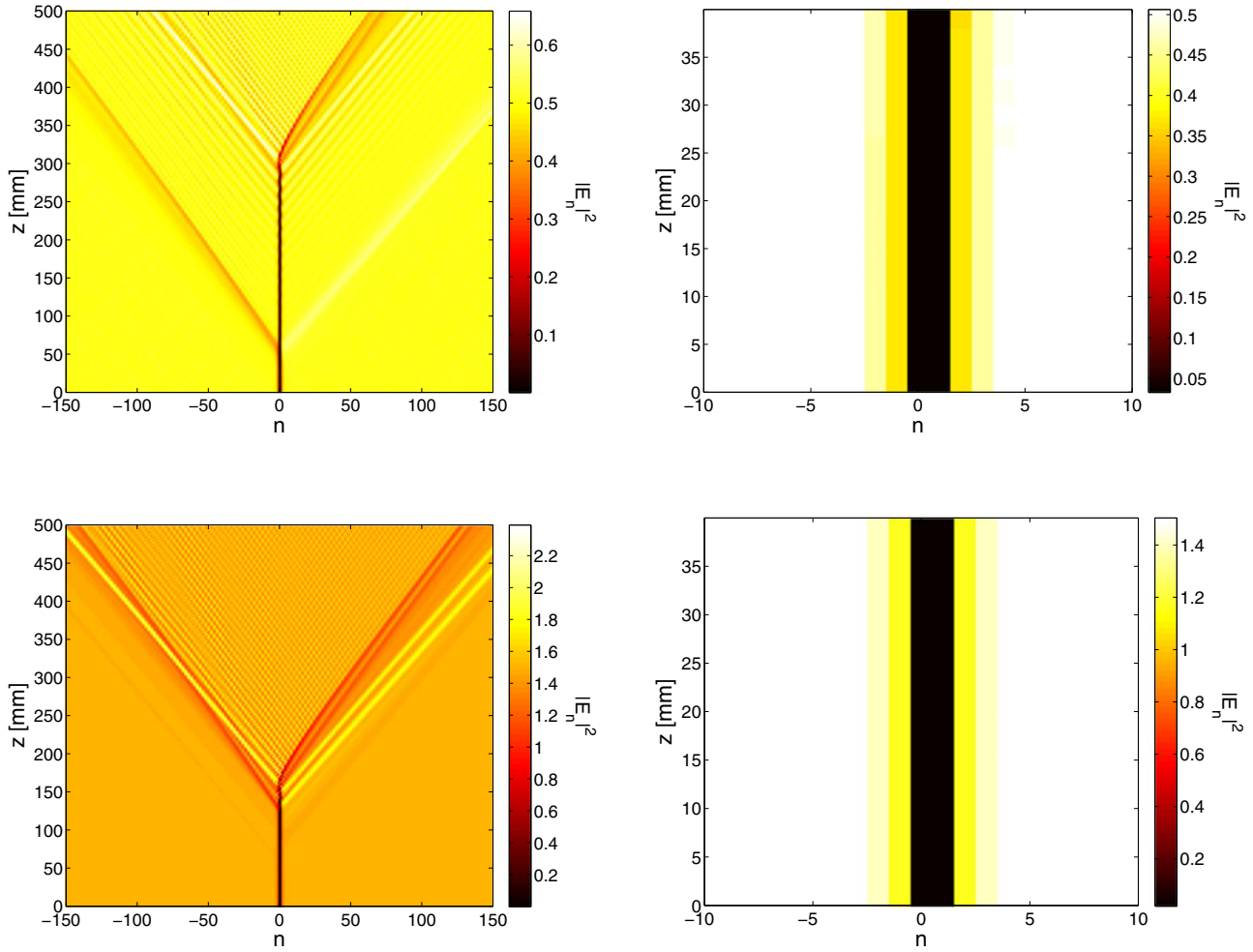

Fig. 9. (Color online) Propagation of the unstable soliton of the top and middle panels of Figure 4 when a random perturbation of amplitude $\sim 10^{-3}$ is introduced. The right panel is a zoom of the left panel, as before. In the left panel, the resolution of the propagation is $z = 0.1$ mm, whereas in the right panel, the resolution is $z = 0.01$ mm.

References

1. Yu.S. Kivshar, B. Luther-Davies, Phys. Rep. **298**, 81 (1998)
2. Yu.S. Kivshar, G.P. Agrawal, *Optical Solitons: From Fibers to Photonic Crystals* (Academic Press San Diego, 2003)
3. D.J. Frantzeskakis, J. Phys. A: Math. Theor. **43**, 213001 (2010)
4. B. Denardo, W. Wright, S. Putterman, A. Larrazza, Phys. Rev. Lett. **64**, 1518 (1990)
5. B. Denardo, B. Galvin, A. Greenfield, A. Larrazza, S. Putterman, W. Wright, Phys. Rev. Lett. **68**, 1730 (1992)
6. L.Q. English, S.G. Wheeler, Y. Shen, G.P. Veldes, N. Whitaker, P.G. Kevrekidis, D.J. Frantzeskakis, Phys. Lett. A **375**, 1242 (2011)
7. M. Chen, M.A. Tsankov, J.M. Nash, C.E. Patton, Phys. Rev. Lett. **70**, 1707 (1993)
8. R. Heidemann, S. Zhdanov, S. Sütterlin, M.H. Thomas, G.E. Morfill, Phys. Rev. Lett. **102**, 135002 (2009)
9. M. Johansson, Yu.S. Kivshar, Phys. Rev. Lett. **82**, 85 (1999)
10. Yu.S. Kivshar, W. Królikowski, O.A. Chubykalo, Phys. Rev. E **50**, 5020 (1994)
11. R. Morandotti, H.S. Eisenberg, Y. Silberberg, M. Sorel, J.S. Aitchison, Phys. Rev. Lett. **86**, 3296 (2001)
12. E. Smirnov, C.E. Rüter, M. Stepić, D. Kip, V. Shandarov, Phys. Rev. E **74**, 065601 (2006)
13. E.P. Fitrakis, P.G. Kevrekidis, H. Susanto, D.J. Frantzeskakis, Phys. Rev. E **75**, 066608 (2007)
14. Lj. Hadzievski, A. Maluckov, M. Stepić, Opt. Exp. **15** (2007) 5687
15. H. Susanto, M. Johansson, Phys. Rev. E **72**, 016605 (2005)
16. D.E. Pelinovsky, P.G. Kevrekidis, J. Phys. A: Math. Theor. **41**, 185206 (2008)
17. P.G. Kevrekidis, *The Discrete Nonlinear Schrödinger Equation*, (Springer-Verlag Heidelberg, 2009)
18. R. Dong, C.E. Rüter, D. Song, J. Xu, D. Kip, Opt. Express **18**, 27493 (2010)
19. R. Dong, C.E. Rüter, D. Kip, J. Cuevas, P.G. Kevrekidis, D. Song, J. Xu, Phys. Rev. A **83**, 063816 (2011)

20. A.A. Sukhorukov, Yu.S. Kivshar, Opt. Lett. **27**, 2112 (2002)
21. R.A. Vicencio, M. Johansson, Phys. Rev. A **79,** 065801 (2009)
22. R. Morandotti, D. Mandelik, Y. Silberberg, J.S. Aitchison, M. Sorel, D.N. Christodoulides, A.A. Sukhorukov, Yu.S. Kivshar, Opt. Lett. **29**, 2890 (2004)
23. A. Kanshu, C.E. Rüter, D. Kip, V. Shandarov, P.P. Beličev, I. Ilić, M. Stepić, Opt. Lett. **37**, 1512 (2012)
24. I.V. Barashenkov, V.G. Makhankov, Phys. Lett. A **128** (1988) 52
25. M. Stepić, C.E. Rüter, D. Kip, A. Maluckov, Lj. Hadzievski, Opt. Commun. **267**, 229 (2006)
26. P.G. Kevrekidis, D.J. Frantzeskakis, R. Carretero-González, B.A. Malomed, A.R. Bishop, Phys. Rev. E **72**, 046613 (2005)
27. I.V. Barashenkov, A.D. Gocheva, V.G. Makhankov, I.V. Puzynin, Phys. D **34**, 240 (1989)
28. I.V. Barashenkov, E.Yu. Panova, Phys. D **69**, 114 (1993)
29. O.F. Oxtoby, I.V. Barashenkov, Phys. Rev. E **76**, 036603 (2007)